Anomalous splitting of the hole states in silicon quantum dots with shallow acceptors

2008 J. Phys.: Condens. Matter 20 025213

(http://iopscience.iop.org/0953-8984/20/2/025213)

J. Phys.: Condens. Matter **20** (2008) 025213 (13pp) doi:10.1088/0953-8984/20/02/025213

Anomalous splitting of the hole states in silicon quantum dots with shallow acceptors

V A Belyakov and V A Burdov

Department of Theoretical Physics, University of Nizhniy Novgorod, Nizhniy Novgorod, 603950, Russia

Received 2 October 2007, in final form 7 November 2007
Published 6 December 2007
Online at stacks.iop.org/JPhysCM/20/025213

Abstract

Hole wavefunctions and energy spectra have been calculated in a silicon quantum dot with a shallow acceptor. Within the framework of the envelope function approach we have found anomalously strong splitting of the energy levels caused by the Coulomb and the spin–orbit interactions as compared to bulk silicon. If the quantum dot has been doped with boron, the short range part of the Coulomb field turns out to be weak, and the long range hydrogenic part plays a crucial role in the energy splitting. In the case where the dot is doped with any other element of the third group, the role of the short range Coulomb interaction becomes determinative. The latter provides stronger energy splitting compared to that in the model of hydrogen-like impurity. In both cases the energy of the splitting substantially exceeds the typical bulk values for these acceptors due to the quantum confinement effect. We have also analysed the charge distribution in the dot and the hole spectrum, depending on the acceptor position inside the nanocrystal.

(Some figures in this article are in colour only in the electronic version)

1. Introduction

Introduction of shallow impurities into silicon quantum dots can strongly modify their electronic structure [1–5] and optical properties [6–13]. Due to the interplay between quantum confinement [14–17] and the microscopic short range Coulomb field (see, e.g., [18–22]) leading to the central cell correction and valley–orbit splitting [23, 24], the dielectric properties of silicon nanocrystals are also modified [25–28]. Manipulation with the dot emittance implies the possibility of controlling the recombination rates of various electron–hole transitions. In turn, control of the recombination rates has been based on knowledge of the wavefunctions of quantum states involved in the recombination process.

The goal of our theoretical analysis is to find the energies and wavefunctions of the ground and several excited hole states of a doped silicon quantum dot. We shall discuss the strong splitting of the energy levels, caused by the hydrogenic and central cell potentials of the impurity ion, and the spin–orbit interaction. In the present paper we consider the case of a shallow acceptor impurity of group III embedded into silicon nanocrystals 2–5 nm in diameter. We shall also study the dependence of the energy spectra and hole density on the nanocrystal size and the acceptor displacement from the dot centre.

For this purpose we employ envelope function approximation, in which the acceptor electrostatic field has a macroscopic long range component and a diagonal microscopic short range one. The latter is introduced in a 'macroscopic' $\mathbf{k}\cdot\mathbf{p}$ Hamiltonian as an additional sharply varied potential [18–22]. Keeping within the framework of a macroscopic picture, it is possible to use the bulk static dielectric constants ε_s and ε_d for materials inside and outside the dot, respectively. As a result, the long range potential, being of hydrogen-like kind in bulk silicon, is modified due to the appearance of polarization charges at the nanocrystal boundary [14–17]. The existence of an excess positive charge near the dot boundary has been confirmed recently by the microscopic first-principles calculations of Lannoo *et al* [26] and Trani *et al* [28].

Note that various questions concerning electronic and optical structure of undoped silicon quantum dots have already been answered in detail earlier; see, e.g., for a review the book of Delerue and Lannoo [29]. At the same time, theoretical study of the impurity states in the dots was not so extensive,

especially for the dots doped with acceptors. The works of Zhou *et al* [2] and Xu *et al* [3] represent some exception. The authors of these papers have calculated binding energies and chemical shifts for group III acceptors in silicon nanocrystals, and found them to be very large compared to those for bulk silicon. However their findings were attributed to very small dots (less than 2 nm in size) with exclusively centrally located acceptors. We present here both analytical and numerical results related to the fine structure of the hole states in p doped silicon quantum dots over a wider range of the dot sizes, and for arbitrary acceptor position inside the dot.

2. Basic equations of the model

We consider a silicon quantum dot of radius R, embedded into a wide band dielectric matrix, and assume, for simplicity, the potential barriers for holes to be infinitely high. The total potential energy of a hole depends not only on the hole position vector $\mathbf{r}$ but also on the acceptor position vector $\mathbf{h}$, and consists of the following four parts:

$$U(\mathbf{r},\mathbf{h}) = U_0(r) + V_{\rm sp}(r) + V_{\rm ih}(\mathbf{r},\mathbf{h}) + W(\mathbf{r},\mathbf{h}). \quad (1)$$

Here $U_0(r)$ is the confining potential equal to zero inside, and infinity outside, the dot.

The second part $V_{\rm sp}(r)$ describes an interaction between the hole and its own image arising due to the charge polarization on the boundary between the silicon nanocrystal and its dielectric surrounding. Since the hole interacts with its own image, the corresponding potential energy is often referred to as a self-polarization term. It can be represented in the form (see, e.g., [15, 29, 30])

$$V_{\rm sp}(r) = -\frac{e^2(\varepsilon_{\rm s}-\varepsilon_{\rm d})}{2\varepsilon_{\rm s}R}\sum_{l=0}^{\infty}\frac{l+1}{l\varepsilon_{\rm s}+(l+1)\varepsilon_{\rm d}}\frac{r^{2l}}{R^{2l}}, \quad (2)$$

where $\varepsilon_{\rm s}$ and $\varepsilon_{\rm d}$ are the static dielectric constants of silicon and the dielectric matrix, respectively. Because we write the self-polarization term for holes, it has an opposite sign with respect to the one for electrons [15, 29, 30].

The third term $V_{\rm ih}(\mathbf{r},\mathbf{h})$ introduced in equation (1) represents a macroscopic hole–ion interaction. It has the form

$$V_{\rm ih}(\mathbf{r},\mathbf{h}) = -\frac{e^2}{\varepsilon_{\rm s}|\mathbf{r}-\mathbf{h}|} - \frac{e^2(\varepsilon_{\rm s}-\varepsilon_{\rm d})}{\varepsilon_{\rm s}R} \times \sum_{l=0}^{\infty}\frac{h^l r^l}{R^{2l}}\frac{l+1}{l\varepsilon_{\rm s}+(l+1)\varepsilon_{\rm d}}P_l(\cos\theta), \quad (3)$$

where θ is the angle between $\mathbf{h}$ and $\mathbf{r}$. The first term corresponds to the direct Coulomb attraction between the acceptor and hole, while the second term describes an interaction between the hole and ion image. This term disappears when $\varepsilon_{\rm s}$ and $\varepsilon_{\rm d}$ become equal.

Finally, $W(\mathbf{r},\mathbf{h})$ is the so-called central cell field [23, 24] arising from the hole–ion interaction as well. However, in contrast to $V_{\rm ih}(\mathbf{r},\mathbf{h})$ reflecting the long range macroscopic part of the Coulomb interaction, the term $W(\mathbf{r},\mathbf{h})$ is the short range contribution that manifests itself at the microscopic level. This field exists in a distance of about the Bohr radius around the acceptor nucleus and, in fact, vanishes at the boundary of the unit cell containing the acceptor. Hence, one may assume the central cell field in a quantum dot to be of the same form as in the bulk. For bulk materials an approximate expression for $W(\mathbf{r},\mathbf{h})$ was obtained earlier from first-principles calculations. Its explicit form is as follows [19, 20]:

$$W(\mathbf{r},\mathbf{h}) = -\frac{e^2}{|\mathbf{r}-\mathbf{h}|} \times \left(A{\rm e}^{-\alpha|\mathbf{r}-\mathbf{h}|} + (1-A){\rm e}^{-\beta|\mathbf{r}-\mathbf{h}|} - \frac{{\rm e}^{-\gamma|\mathbf{r}-\mathbf{h}|}}{\varepsilon_{\rm s}}\right), \quad (4)$$

where α, β, γ, and A are some fitting parameters. Their values vary within about twenty per cent related to $0.755/a_{\rm B}$, $0.35/a_{\rm B}$, $2.45/a_{\rm B}$, and 1.14, respectively, depending on the experimental data set to be used [19]. Here $a_{\rm B}$ stands for the Bohr radius.

In what follows, we shall calculate several lower hole energy levels and wavefunctions in a silicon quantum dot doped with an acceptor. We shall also find the splitting of the hole spectrum caused by the spin–orbit interaction and electric field of acceptor in the case where the latter occupies some arbitrary asymmetric position inside the dot. To this end we are going to exploit here the envelope function approximation ($\mathbf{k}\cdot\mathbf{p}$ method) whose applicability to 2–5 nm silicon nanocrystals has been confirmed earlier in a lot of publications; see, e.g., [4, 5, 31–35].

To find the hole states we have to solve a single-particle Schrödinger-like equation of the following kind:

$$(H + \bar{U}(\mathbf{r},\mathbf{h}))|\Phi\rangle = E|\Phi\rangle. \quad (5)$$

Here, H is the bulk $\mathbf{k}\cdot\mathbf{p}$ Hamiltonian operator acting in the space of the six-dimensional (6D) envelope function vectors $|\Phi\rangle$, and E stands for the hole energy. Components of the 6D vector $|\Phi\rangle$ are slowly varied expansion coefficients $\Phi_j(\mathbf{r})$ of the total wavefunction in the Bloch state basis of a Γ point: $|YZ\rangle|\uparrow\rangle$, $|XZ\rangle|\uparrow\rangle$, $|XY\rangle|\uparrow\rangle$, $|YZ\rangle|\downarrow\rangle$, $|XZ\rangle|\downarrow\rangle$, $|XY\rangle|\downarrow\rangle$, where $|\uparrow\rangle$ and $|\downarrow\rangle$ are 'up' and 'down' spinors, respectively, and the Bloch functions $|YZ\rangle$, $|XZ\rangle$, $|XY\rangle$ belong to the irreducible representation $\Gamma_{25'}$. The functional operator $\bar{U}(\mathbf{r},\mathbf{h})$, introduced in equation (5), differs from $U(\mathbf{r},\mathbf{h})$ defined before with equation (1).

As usual, when obtaining the $\mathbf{k}\cdot\mathbf{p}$ Hamiltonian we have to multiply the single-particle Schrödinger equation by any conjugate Bloch function and then integrate the equation obtained over the unit-cell volume Ω. As a consequence, all the external fields appear in the $\mathbf{k}\cdot\mathbf{p}$ Hamiltonian in some averaged form.

Since the long range part of the Coulomb interaction $V_{\rm sp}(r) + V_{\rm ih}(\mathbf{r},\mathbf{h})$ is a smooth function, it is strictly diagonal in the Bloch state basis. The averaging over the unit-cell volume does not change this function which gives rise in diagonal elements of the $\mathbf{k}\cdot\mathbf{p}$ Hamiltonian.

The central cell potential $W(\mathbf{r},\mathbf{h})$ varies sharply and, generally speaking, can connect Bloch states corresponding to essentially different wavevectors in a Brillouin zone, as it takes place in a conduction band of silicon [23, 24]. However, because of the isotropic form of the function $W(\mathbf{r},\mathbf{h})$ with respect to the acceptor site and $\Gamma_{25'}$ symmetry of the Bloch

functions, one can conclude that the short range potential, as well as the long range one, will contribute only to the diagonal elements of the $\mathbf{k}\cdot\mathbf{p}$ matrix. At the same time the short range field crucially changes its form in the $\mathbf{k}\cdot\mathbf{p}$ Hamiltonian compared to that in equation (4). As has already been pointed out, averaging $W(\mathbf{r},\mathbf{h})$ over the unit cell yields, in fact, a nonzero value only for the unit cell containing the acceptor. Consequently, the short range diagonal elements may be approximated by the Dirac δ function

$$\bar{W} \equiv \langle YZ|\,W(\mathbf{r},\mathbf{h})|YZ\rangle_\Omega = \langle XZ|\,W(\mathbf{r},\mathbf{h})|XZ\rangle_\Omega = \langle XY|\,W(\mathbf{r},\mathbf{h})|XY\rangle_\Omega = -Q\delta(\mathbf{r}-\mathbf{h}), \tag{6}$$

as has been done earlier for donors in silicon nanocrystals [4, 5, 36] and layers [37]. Here, $\langle A|\,W|B\rangle_\Omega \equiv \Omega^{-1}\int_\Omega A^*(\mathbf{r})W(\mathbf{h},\mathbf{r})B(\mathbf{r})\,\mathrm{d}\mathbf{r}$, and Q is some parameter independent of $\mathbf{r}$ and $\mathbf{h}$, which can be determined from experimental data for the acceptor energy levels in bulk silicon.

It is known that the experimentally observed binding energies for group III acceptors (except for boron) in bulk silicon strongly differ from those obtained theoretically within the framework of the hydrogen-like model [21, 38, 39]. For example, the experimental value of the binding energy for aluminium equals 68.9 meV, while the calculated value, which is the same for all hydrogen-like acceptors, is substantially less and equals 44.4 meV according to the latest results of Lipari and Baldereschi [21]. The difference may be attributed to the short range potential that should be, obviously, taken into account.

Let us denote the experimentally observed energy shift of the acceptor binding energy related to the theoretically calculated value (44.4 meV) as η. Then the number Q can be expressed through η similarly to the method suggested earlier for donors [36, 37]. This yields an approximate expression: $Q = \pi(a^*)^3\eta$, where $a^* = \hbar^2\varepsilon_\mathrm{s}/m^*e^2$ is the analogue of the hole effective Bohr radius. The definition of m^* and the explanation of why a^* does not coincide with the true hole effective Bohr radius $a_\mathrm{h} \equiv \hbar^2\varepsilon_\mathrm{s}/m_\mathrm{h}e^2$ will be given a little later. Thus, the function $\bar{U}(\mathbf{r},\mathbf{h})$ is represented as follows: $\bar{U}(\mathbf{r},\mathbf{h}) = U_0(r) + V_\mathrm{sp}(r) + V_\mathrm{ih}(\mathbf{r},\mathbf{h}) - Q\delta(\mathbf{r}-\mathbf{h})$.

It is convenient to write the $\mathbf{k}\cdot\mathbf{p}$ Hamiltonian matrix H in equation (5) for holes as the sum of three parts: $H = H^{(0)} + H^{(1)} + H^{(\mathrm{so})}$. Here $H^{(0)} = (\mathbf{p}^2/2m_\mathrm{h})\times\mathbf{I}$ is the isotropic part obtained as the average of the total $\mathbf{k}\cdot\mathbf{p}$ matrix over angles in the $\mathbf{p}$ space, $\mathbf{I}$ stands for the 6×6 identity matrix, the hole effective mass $m_\mathrm{h} = 3m_0/(L+2M)$, where the numbers L, M, N are some dimensionless empirical parameters of the $\mathbf{k}\cdot\mathbf{p}$ Hamiltonian operator in a valence band. For silicon they equal 5.8, 3.43, 8.61, respectively [40]. $H^{(1)}$ is the anisotropic part that can be represented by two equivalent blocks 3×3 situated on a leading diagonal of the total 6×6 $\mathbf{k}\cdot\mathbf{p}$ matrix:

$$H^{(1)} = \begin{pmatrix} H_3 & 0 \\ 0 & H_3 \end{pmatrix},$$

$$H_3 = \frac{1}{2m_0}\begin{pmatrix} \frac{L-M}{3}(3p_x^2-\mathbf{p}^2) & Np_xp_y & Np_xp_z \\ Np_xp_y & \frac{L-M}{3}(3p_y^2-\mathbf{p}^2) & Np_yp_z \\ Np_xp_z & Np_yp_z & \frac{L-M}{3}(3p_z^2-\mathbf{p}^2) \end{pmatrix}. \tag{7}$$

Finally, the term $H^{(\mathrm{so})}$ describes the spin–orbit interaction. For holes it is written as

$$H^{(\mathrm{so})} = \tfrac{1}{3}\begin{pmatrix} 0 & \mathrm{i}\Delta & 0 & 0 & 0 & -\Delta \\ -\mathrm{i}\Delta & 0 & 0 & 0 & 0 & \mathrm{i}\Delta \\ 0 & 0 & 0 & \Delta & -\mathrm{i}\Delta & 0 \\ 0 & 0 & \Delta & 0 & -\mathrm{i}\Delta & 0 \\ 0 & 0 & \mathrm{i}\Delta & \mathrm{i}\Delta & 0 & 0 \\ -\Delta & -\mathrm{i}\Delta & 0 & 0 & 0 & 0 \end{pmatrix}. \tag{8}$$

We have introduced above the spin–orbit energy Δ equal to 44 meV for silicon.

Let us now return to the inequality $m^* \neq m_\mathrm{h}$, and, consequently, $a^* \neq a_\mathrm{h}$, and briefly discuss this problem. Strictly speaking, in order to apply the procedure of determination of Q through the shift η similarly to the one proposed earlier [4, 5, 36, 37], we have to use the bulk-like envelope function $\Phi(\mathbf{r})$ in the equality $Q|\Phi(0)|^2 = \eta$. In the case of the single band, $\Phi(\mathbf{r})$, as a rule, represents the 1s function of the hydrogen-like ground state with the normalization constant $(\pi a^3)^{-1/2}$, where a stands for the effective Bohr radius of the single-band problem. Therefore the parameter Q may be written as $\pi a^3\eta$. However, as has been shown by Lipari and Baldereschi [21, 38, 39], the single-band model is insufficient to provide a required accuracy in a binding energy of the hydrogenic acceptor. According to their analysis [21], the six-band model with envelope functions being the expansions over the spherical harmonics up to the orbital quantum number $l = 8$ has to be considered in order to achieve the needed accuracy. Correspondingly, instead of the simple relationship between Q and η, typical for the single-band model, we shall obtain some cumbersome expression including normalization coefficients of all the s-type hydrogenic envelope functions (at least from 1s to 8s) with their weight coefficients which come from the expansion of the envelope functions over the spherical harmonics.

At the same time, since the energy of the acceptor state lies above the energy maximum within the band gap, it seems to be quite logical to suppose that this state forms predominantly from the heavy holes with the greater value of the effective mass and smaller value of the effective Bohr radius than m_h and a_h, respectively. On this basis we may, presumably, replace the cumbersome expansion over the spherical harmonics of Lipari and Baldereschi by the single 1s-type hydrogen-like envelope function with some other value of the effective Bohr radius a^*. The effective mass m^* in the expression for a^* should be chosen so that the correct value of the binding energy 44.4 meV [21] could be obtained. Indeed, this value turns out to be very close to the heavy hole effective mass (theoretically calculated value $0.45m_0$) and equals 0.42 times the free electron mass. The Bohr radius a^* equals $0.635a_\mathrm{h}$ in this case.

It is important to note that the boron acceptor takes a special position in our consideration. Since the experimental value of the binding energy for boron completely coincides [21] with that obtained within the hydrogen-like model (44.4 meV), the parameter Q turns out to be zero in this case. This means that the central cell field will not contribute to the hole spectrum and wavefunctions of the B doped dot. As

a consequence, boron may be treated as a hydrogenic acceptor. It does not take place for all the other group III acceptors: Al, Ga, In, and Tl. As has been already pointed out, the energy shift η is sufficiently great for these acceptors and equals 24.5 meV, 28.3 meV, 111.8 meV, and 203.3 meV [22], respectively. No doubt the central cell field will play a crucial role in the hole state formation for a silicon nanocrystal doped with these acceptors. On this basis, solving the basic equation (5) will be carried out separately for these two different kinds of acceptors.

Let us discuss the approach to solving equation (5), which is valid for all kinds of acceptors. Because of the isotropic and diagonal form of the operator $H^{(0)}+U_0(r)$, its eigenstates may be classified similarly to atomic systems as the states of s, p, d type, etc [33]. Accordingly, one may expand the components of the envelope function vectors $|\Phi\rangle$ over the proper basis of $H^{(0)}+U_0(r)$ as

$$\Phi_j(\mathbf{r}) = \sum_\alpha C_{j\alpha}|\alpha\rangle, \tag{9}$$

where $|\alpha\rangle$ denote the s, p, d, ... eigenstates of the operator $H^{(0)}+U_0(r)$, and $C_{j\alpha}$ are the expansion coefficients. For convenience, we choose the vectors $|\alpha\rangle$ as real functions with the symmetry of x, y, or z type (for p-type states), xy, xz, yz, x^2-y^2, or $\mathbf{r}^2-3z^2$ type (for d-type states), etc. Substitution of $\Phi_j(\mathbf{r})$ into equation (5) yields algebraic equations for $C_{j\alpha}$:

$$(E-E_\alpha)C_{i\alpha} = \sum_\beta \langle\alpha|H_{ij}^{(1)}+H_{ij}^{(\mathrm{so})}+V(\mathbf{r},\mathbf{h})\delta_{ij}|\beta\rangle C_{j\beta}. \tag{10}$$

Here $V(\mathbf{r},\mathbf{h}) = V_{\mathrm{sp}}(r)+V_{\mathrm{ih}}(\mathbf{r},\mathbf{h})+\bar{W}$ is the Coulomb potential energy, δ_{ij} stands for the Kronecker delta, and Einstein convention has been used when summing over j. E_α denotes the energy of the state $|\alpha\rangle$, i.e. the eigenvalue of the operator $H^{(0)}+U_0(r)$. For instance, s- and p-type states have the energies $E_{\mathrm{s}} = \hbar^2\pi^2/2m_{\mathrm{h}}R^2$ and $E_{\mathrm{p}} = \hbar^2\mu^2/2m_{\mathrm{h}}R^2$, where $\mu = 4.4934$ is the first root of the spherical Bessel function $j_1(x)$. In the simplest case of no spin–orbit and Coulomb interactions, one can obtain several low energy hole states in the quantum dot, if we restrict ourselves to the 1s-, 1p-, 1d-type (s-, p-, d-type states in the following), and 2s-type states only in equations (9) and (10).

In figure 1 the energies of several hole states have been plotted as functions of the dot radius. It is seen that two lower hole levels have very close energies. The lowest level, being sixfold degenerate, has the energy $E_{0\mathrm{h}} = E_{\mathrm{s}}$ and corresponds to six electron states with the s-type envelope function. The second level corresponds to six electron states with the p-type envelope functions and the energy $E_{1\mathrm{h}} = E_{\mathrm{p}}\left[1-(3N+2L-2M)/(5L+10M)\right]$. Like the other three levels, shown in the figure with short dashed lines, this one has been obtained as a result of the p–p hybridization. Dotted lines represent the d–d hybridized energy levels, and the d–2s hybridized levels are represented with long dashed lines. A similar structure of the hole spectrum was found earlier [33, 35] within the framework of the $\mathbf{k}\cdot\mathbf{p}$ method for undoped silicon nanocrystals.

As is shown in figure 1, the two lowest levels are well separated from the other ones shifted up by the distance

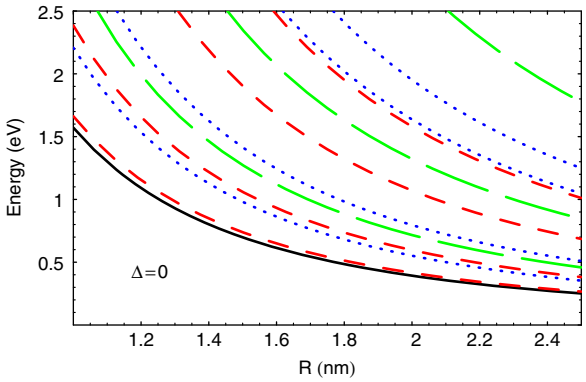

Figure 1. Energy spectrum of the undoped dot at the zeroth spin–orbit splitting. Solid line: s-type level. Short dashed lines: p–p hybridized levels. Dots: d–d hybridized levels. Long dashed lines: 2s–d hybridized levels. The degeneracy degree (from bottom to top): 6; 6; 6; 4; 6; 4; 6; 6; 2; 6; 2; 6.

substantially exceeding the magnitude of the Coulomb or spin–orbit energy. On this basis, electron states of all the upper levels weakly mix with the states of the energies $E_{0\mathrm{h}}$ and $E_{1\mathrm{h}}$. Therefore, these upper states will not contribute, in fact, to the spectrum splitting at the bottom of the hole 'energy band'. Consequently, we may omit them from our further consideration. In contrast, twelve states with the energies $E_{0\mathrm{h}}$ and $E_{1\mathrm{h}}$ will be efficiently mixed due to the Coulomb and spin–orbit interactions forming some fine structure of the spectrum. In the following we restrict ourselves to these states only and investigate their splitting.

3. The 'zoology'

First, we take into account the spin–orbit coupling. As is known, diagonalization of the matrix $H^{(\mathrm{so})}$ with the six Luttinger functions [41] of the angular momentum $J = 3/2$ and $J = 1/2$ gives fourfold and twofold hole levels with the energies $-\Delta/3$ and $2\Delta/3$, respectively. This property of the spin–orbit interaction remains valid for quantum dots as well. Diagonalization of the Hamiltonian matrix $H+U_0(r)$ within the restricted basis of the twelve hole states yields two fourfold and two twofold energies, as is shown in figure 2 with solid lines. For the six states having the s-type envelope function with the orbital momentum $l = 0$, the energies are $E_{0\mathrm{h}}^{(0)} = E_{0\mathrm{h}}-\Delta/3$ for the quadruplet, and $E_{0\mathrm{h}}^{(1)} = E_{0\mathrm{h}}+2\Delta/3$ for the doublet. The states with the p-type envelope function ($l = 1$) have the energy of the splitting two times less. In particular, the quadruplet has the energy $E_{1\mathrm{h}}^{(0)} = E_{1\mathrm{h}}-\Delta/6$, while the energy of the doublet is $E_{1\mathrm{h}}^{(1)} = E_{1\mathrm{h}}+\Delta/3$. Because of the spectrum degeneracy, the wavefunctions may be chosen to a certain extent arbitrarily. Nevertheless, it is more convenient to classify the wavefunctions of the electron states obtained over the eigenvalues of different angular momentum operators of the problem. Below we adduce this classification.

In the case of no Coulomb interaction ($V(\mathbf{r},\mathbf{h}) \to 0$ in equation (10)), the Hamiltonian $\mathbf{k}\cdot\mathbf{p}$ matrix $H^{(0)}+H^{(1)}+H^{(\mathrm{so})}+U_0(r)$ can be formally written in the basis of the twelve 6D envelope function vectors being

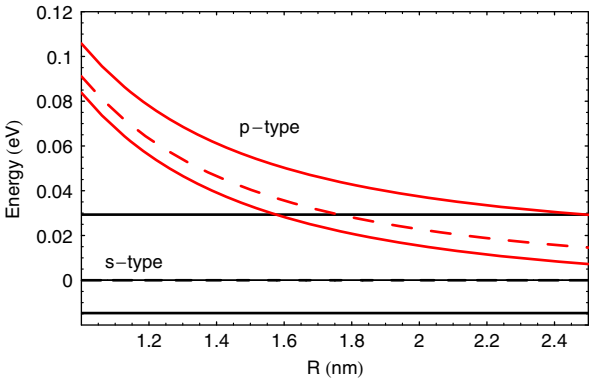

Figure 2. Spin–orbit splitting of the two lowest levels versus the dot radius. The energies of the split levels of the s-type $E_{0h}^{(0,1)}$ (lower parallel solid lines) and p-type $E_{1h}^{(0,1)}$ levels (upper parallel solid lines) have been plotted relative to the lowest unperturbed s-type level (lower dashed line). The upper dashed line indicates the upper unperturbed p-type level. The lower s-type and p-type levels are fourfold degenerate. The upper s-type and p-type levels represent the doublet energies.

the solutions of equation (10) with the energies $E_{0h}^{(0,1)}$ and $E_{1h}^{(0,1)}$:

$$H = \sum_{m=1}^{12} |\Phi^{(m)}\rangle E^{(m)} \langle \Phi^{(m)}|, \tag{11}$$

where $E^{(m)}$ stands for $E_{0h}^{(0,1)}$ and $E_{1h}^{(0,1)}$. Straightforward calculation shows that the Hamiltonian matrix H commutes with the following momentum operators: $\mathbf{I}^2$, $\mathbf{S}^2$, $\mathbf{l}^2$, $\mathbf{K}^2$, K_z, $\mathbf{F}^2$, F_z, which form the complete set. Here $\mathbf{I}$ and $\mathbf{l}$ are orbital moments of the Bloch [41] and envelope functions, respectively, $\mathbf{S}$ stands for spin, and $\mathbf{K} = \mathbf{I} + \mathbf{l}$ is the total orbital momentum of the hole state. Finally, $\mathbf{F} = \mathbf{I} + \mathbf{l} + \mathbf{S}$ is the total angular momentum which was introduced earlier by many authors; see, e.g., [42–45] for A_2B_6, [34, 35] for silicon, and [46] for A_3B_5 quantum dots. In a certain sense operators $\mathbf{I}^2$ and $\mathbf{S}^2$ are trivial, because they represent identity matrices. All the other operators are nontrivial. Correspondingly, electron states belonging to a certain degenerate energy level may differ from each other by some quantum numbers from the above complete set. Let us denote these numbers, excluding the former two, as l, K, K_z, F, F_z, respectively. It is seen that the Luttinger quantum numbers J and J_z corresponding to the total angular momentum of a Bloch state are no longer good quantum numbers because of the appearance of states with the p-type envelope functions.

The wavefunctions of all the twelve states are characterized with the six nontrivial quantum numbers, if the principal quantum number defining an energy level is taken into account. However we shall characterize the eigenfunctions, for simplicity, with only three numbers: F, F_z, and l, which unambiguously define each of the obtained electron states. Accordingly, the 6D envelope function vectors $|\Phi^{(m)}\rangle$ describing these states will be denoted as $|F; F_z; l\rangle$. As a result, the s-type quadruplet with the energy $E_{0h}^{(0)}$ is defined by the following vectors:

$$\left|\frac{3}{2};\frac{3}{2};0\right\rangle = -\frac{|s\rangle}{\sqrt{2}}\begin{pmatrix}1\\ \mathrm{i}\\ 0\\ 0\\ 0\\ 0\end{pmatrix}, \quad \left|\frac{3}{2};-\frac{3}{2};0\right\rangle = \frac{|s\rangle}{\sqrt{2}}\begin{pmatrix}0\\ 0\\ 0\\ 1\\ -\mathrm{i}\\ 0\end{pmatrix},$$
$$\left|\frac{3}{2};\frac{1}{2};0\right\rangle = -\frac{|s\rangle}{\sqrt{6}}\begin{pmatrix}0\\ 0\\ -2\\ 1\\ \mathrm{i}\\ 0\end{pmatrix}, \quad \left|\frac{3}{2};-\frac{1}{2};0\right\rangle = \frac{|s\rangle}{\sqrt{6}}\begin{pmatrix}1\\ -\mathrm{i}\\ 0\\ 0\\ 0\\ 2\end{pmatrix}, \tag{12}$$

while 6D vectors of the s-type doublet (the energy $E_{0h}^{(1)}$) have the form

$$\left|\frac{1}{2};\frac{1}{2};0\right\rangle = -\frac{|s\rangle}{\sqrt{3}}\begin{pmatrix}0\\ 0\\ 1\\ 1\\ \mathrm{i}\\ 0\end{pmatrix}, \quad \left|\frac{1}{2};-\frac{1}{2};0\right\rangle = \frac{|s\rangle}{\sqrt{3}}\begin{pmatrix}1\\ -\mathrm{i}\\ 0\\ 0\\ 0\\ -1\end{pmatrix}. \tag{13}$$

The Bloch functions of all these states coincide with the six Luttinger functions of the momentum $J = 3/2$ and $J = 1/2$. It is not so for the other six states, whose wavefunctions may not be represented as the product of one of the Luttinger functions and p-type envelope function. They have symmetry that is similar to that of the above six states; however the quantum number l equals now 1.

The wavefunctions of the p-type quadruplet (the energy $E_{1h}^{(0)}$) are defined with the vectors

$$\left|\frac{3}{2};\frac{3}{2};1\right\rangle = \frac{1}{2}\begin{pmatrix}-\mathrm{i}|p_z\rangle\\ |p_z\rangle\\ \mathrm{i}|p_x\rangle - |p_y\rangle\\ 0\\ 0\\ 0\end{pmatrix},$$
$$\left|\frac{3}{2};-\frac{3}{2};1\right\rangle = \frac{1}{2}\begin{pmatrix}0\\ 0\\ 0\\ -\mathrm{i}|p_z\rangle\\ -|p_z\rangle\\ \mathrm{i}|p_x\rangle + |p_y\rangle\end{pmatrix},$$
$$\left|\frac{3}{2};\frac{1}{2};1\right\rangle = \frac{1}{2\sqrt{3}}\begin{pmatrix}-2|p_y\rangle\\ 2|p_x\rangle\\ 0\\ -\mathrm{i}|p_z\rangle\\ |p_z\rangle\\ \mathrm{i}|p_x\rangle - |p_y\rangle\end{pmatrix}, \tag{14}$$
$$\left|\frac{3}{2};-\frac{1}{2};1\right\rangle = \frac{1}{2\sqrt{3}}\begin{pmatrix}-\mathrm{i}|p_z\rangle\\ -|p_z\rangle\\ \mathrm{i}|p_x\rangle + |p_y\rangle\\ -2|p_y\rangle\\ 2|p_x\rangle\\ 0\end{pmatrix}.$$

Finally, the wavefunctions of the p-type doublet (the energy $E_{1h}^{(1)}$) are as follows:

$$\left|\frac{1}{2};\frac{1}{2};1\right\rangle = \frac{1}{\sqrt{6}}\begin{pmatrix} |p_y\rangle \\ -|p_x\rangle \\ 0 \\ -\mathrm{i}|p_z\rangle \\ |p_z\rangle \\ \mathrm{i}|p_x\rangle - |p_y\rangle \end{pmatrix},$$
$$\left|\frac{1}{2};-\frac{1}{2};1\right\rangle = \frac{1}{\sqrt{6}}\begin{pmatrix} -\mathrm{i}|p_z\rangle \\ -|p_z\rangle \\ \mathrm{i}|p_x\rangle + |p_y\rangle \\ |p_y\rangle \\ -|p_x\rangle \\ 0 \end{pmatrix}. \tag{15}$$

Despite the fact that the functions with $l = 1$ are not eigenfunctions of the Luttinger momentum operators $\mathbf{J}^2$ and J_z, the matrix of the spin–orbit interaction is rigorously diagonal in a basis of these functions.

4. Hole states in a nanocrystal with an acceptor

Now we can do the last step and take into account the Coulomb field. Existence of the impurity in the nanocrystal will result in a mixing of the twelve electron states (equations (12)–(15)). It is possible to expand the 6D envelope function vector $|\Phi\rangle$ for the doped dot over the states $|F;F_z;l\rangle$ as

$$|\Phi\rangle = \sum_{F=1/2}^{3/2}\sum_{F_z=-F}^{F}\sum_{l=0}^{1} f_{F,F_z,l}|F;F_z;l\rangle, \tag{16}$$

where $f_{F,F_z,l}$ are constant expansion coefficients being the solutions of the eigenstate and eigenvalue problem

$$(E - E_{F,F_z,l})f_{F,F_z,l} = \sum_{G=1/2}^{3/2}\sum_{G_z=-G}^{G}\sum_{n=0}^{1}\langle F;F_z;l|\,V(\mathbf{r})|G;G_z;n\rangle f_{G,G_z,n}, \tag{17}$$

where E is an eigenvalue to be determined.

The solution of equation (17) depends on the explicit form of $V(\mathbf{r})$ that is different for hydrogenic and real acceptors creating the central cell field. We first consider the situation with the hydrogen-like (boron) acceptor.

4.1. Hydrogen-like acceptor

Solving equation (17) gives the following results. The energy spectrum develops into a fine structure consisting of the six close doubly degenerate levels. Two energies of the six can be found analytically from equation (17). As will be established later, these two energies correspond to the ground state doublet (the energy E_0) and the doublet of the fourth excited state (the energy E_4):

$$E_{0,4} = \left\{E_{0h}^{(0)}(q) + E_{1h}^{(0)}(q) \pm \sqrt{(E_{0h}^{(0)}(q) - E_{1h}^{(0)}(q))^2 + 2V^2(q)}\right\}\{2\}^{-1}, \tag{18}$$

where $V^2(q) = V_x^2(q) + V_y^2(q) + V_z^2(q)$, $E_{0h}^{(0,1)}(q) = E_{0h}^{(0,1)} + V_{ss}(q)$, $E_{1h}^{(0,1)}(q) = E_{1h}^{(0,1)} + V_{pp}(q)$, $q = h/R$. The minus sign stands for E_0, and the plus sign stands for E_4. We have introduced also matrix elements of the Coulomb potential energy $V_a(q) \equiv \langle s|V_{sp}(r) + V_{ih}(\mathbf{r},\mathbf{h})|p_a\rangle$, $V_{ss}(q) \equiv \langle s|V_{sp}(r) + V_{ih}(\mathbf{r},\mathbf{h})|s\rangle$, and $V_{pp}(q) \equiv \langle\langle p_a|V_{sp}(r) + V_{ih}(\mathbf{r},\mathbf{h})|p_a\rangle\rangle$ for the case where $\bar{W} = 0$. It should be noted that the Coulomb matrix elements of $p_a - p_a$ type have some anisotropic addition proportional to $q^2 - 3q_a^2$. However, it is negligibly small compared to the isotropic average part denoted here as $V_{pp}(q)$.

The wavefunctions of the lowest doublet with the energy E_0 may be defined by the following orthonormal 6D vectors:

$$\begin{aligned}|\Phi_0^{(1)}\rangle = -\frac{\sin\beta}{h}\Bigg(&\mathrm{i}\frac{h_z h_+}{h_\perp}\left|\frac{3}{2};\frac{3}{2};1\right\rangle - \frac{\sqrt{3}}{2}h_\perp\left|\frac{3}{2};\frac{1}{2};1\right\rangle \\ &+ \frac{h_-^2}{2h_\perp}\left|\frac{3}{2};-\frac{3}{2};1\right\rangle\Bigg) + \frac{\cos\beta}{h^2}\Bigg(-\frac{h_+(h_z^2+h^2)}{2h_\perp} \\ &\times\left|\frac{3}{2};\frac{3}{2};0\right\rangle - \mathrm{i}\frac{\sqrt{3}}{2}h_z h_\perp\left|\frac{3}{2};\frac{1}{2};0\right\rangle \\ &+ \frac{\sqrt{3}}{2}h_- h_\perp\left|\frac{3}{2};-\frac{1}{2};0\right\rangle - \frac{\mathrm{i}}{2}\frac{h_z h_-^2}{h_\perp}\left|\frac{3}{2};-\frac{3}{2};0\right\rangle\Bigg), \\ |\Phi_0^{(2)}\rangle = -\frac{\sin\beta}{h}\Bigg(&\frac{h_+^2}{2h_\perp}\left|\frac{3}{2};\frac{3}{2};1\right\rangle - \frac{\sqrt{3}}{2}h_\perp\left|\frac{3}{2};-\frac{1}{2};1\right\rangle \\ &+ \mathrm{i}\frac{h_z h_-}{h_\perp}\left|\frac{3}{2};-\frac{3}{2};1\right\rangle\Bigg) + \frac{\cos\beta}{h^2}\Bigg(\frac{\mathrm{i}}{2}\frac{h_z h_+^2}{h_\perp}\left|\frac{3}{2};\frac{3}{2};0\right\rangle \\ &- \frac{\sqrt{3}}{2}h_+ h_\perp\left|\frac{3}{2};\frac{1}{2};0\right\rangle + \mathrm{i}\frac{\sqrt{3}}{2}h_z h_\perp\left|\frac{3}{2};-\frac{1}{2};0\right\rangle \\ &+ \frac{h_-(h_z^2+h^2)}{2h_\perp}\left|\frac{3}{2};-\frac{3}{2};0\right\rangle\Bigg).\end{aligned} \tag{19}$$

Correspondingly, the vectors of envelope functions of the doublet with the energy E_4 may be chosen as

$$\begin{aligned}|\Phi_4^{(1)}\rangle = \frac{\cos\beta}{h}\Bigg(&\mathrm{i}\frac{h_z h_+}{h_\perp}\left|\frac{3}{2};\frac{3}{2};1\right\rangle - \frac{\sqrt{3}}{2}h_\perp\left|\frac{3}{2};\frac{1}{2};1\right\rangle \\ &+ \frac{h_-^2}{2h_\perp}\left|\frac{3}{2};-\frac{3}{2};1\right\rangle\Bigg) + \frac{\sin\beta}{h^2}\Bigg(-\frac{h_+(h_z^2+h^2)}{2h_\perp}\left|\frac{3}{2};\frac{3}{2};0\right\rangle \\ &- \mathrm{i}\frac{\sqrt{3}}{2}h_z h_\perp\left|\frac{3}{2};\frac{1}{2};0\right\rangle + \frac{\sqrt{3}}{2}h_- h_\perp\left|\frac{3}{2};-\frac{1}{2};0\right\rangle \\ &- \frac{\mathrm{i}}{2}\frac{h_z h_-^2}{h_\perp}\left|\frac{3}{2};-\frac{3}{2};0\right\rangle\Bigg), \\ |\Phi_4^{(2)}\rangle = \frac{\cos\beta}{h}\Bigg(&\frac{h_+^2}{2h_\perp}\left|\frac{3}{2};\frac{3}{2};1\right\rangle - \frac{\sqrt{3}}{2}h_\perp\left|\frac{3}{2};-\frac{1}{2};1\right\rangle \\ &+ \mathrm{i}\frac{h_z h_-}{h_\perp}\left|\frac{3}{2};-\frac{3}{2};1\right\rangle\Bigg) + \frac{\sin\beta}{h^2}\Bigg(\frac{\mathrm{i}}{2}\frac{h_z h_+^2}{h_\perp}\left|\frac{3}{2};\frac{3}{2};0\right\rangle \\ &- \frac{\sqrt{3}}{2}h_+ h_\perp\left|\frac{3}{2};\frac{1}{2};0\right\rangle + \mathrm{i}\frac{\sqrt{3}}{2}h_z h_\perp\left|\frac{3}{2};-\frac{1}{2};0\right\rangle \\ &+ \frac{h_-(h_z^2+h^2)}{2h_\perp}\left|\frac{3}{2};-\frac{3}{2};0\right\rangle\Bigg).\end{aligned} \tag{20}$$

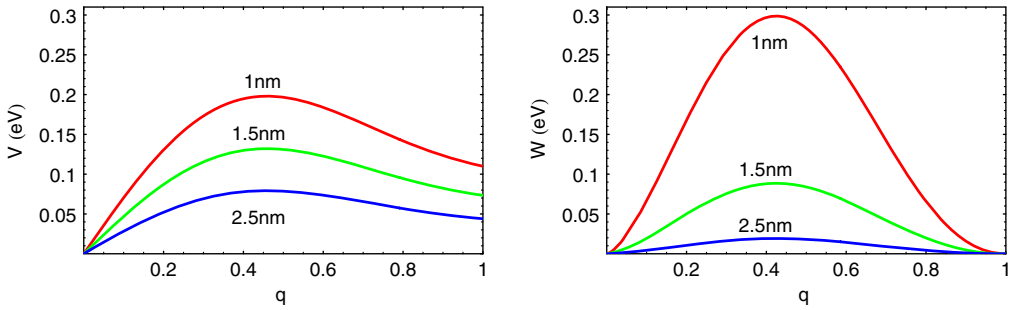

Figure 3. s–p-type matrix elements $V(q)$ and $W(q)$ of the long and short range Coulomb potential energies, respectively, depending on q. Numbers near the curves indicate the dot radius. It is seen that increase of $V(q)$ and $W(q)$ correlates with decrease of the 'weight' (see figure 4).

Here $h^2 = h_x^2 + h_y^2 + h_z^2$, $h_\perp^2 = h_x^2 + h_y^2$, $h_\pm = h_y \pm ih_x$, and the angle β is defined by

$$\cos 2\beta = \frac{E_{1h}(q) - E_{0h}(q)}{\sqrt{(E_{1h}(q) - E_{0h}(q))^2 + 2V^2(q)}}, \qquad (21)$$

where $E_{0h}(q) = E_{0h} + V_{ss}(q)$, and $E_{1h}(q) = E_{1h} + V_{pp}(q)$. It is seen that F remains a good quantum number in the states $|\Phi_{0,4}^{(1,2)}\rangle$, in contrast to F_z and l.

However, it is not so for the other eight electron states. As the numerical calculations show, the envelope function 6D vectors (equation (16)) for these states are superpositions of all the twelve vectors $|F; F_z; l\rangle$, including also the vectors with $F = 1/2$. Evidently, F cannot be a good quantum number for such superpositions. The only physical quantity that has a defined value for all the states, independently of the impurity position inside the nanocrystal, is the squared total orbital momentum $\mathbf{K}^2$. Its value equals unity for all the states. This is a consequence of us using the strongly simplified model in which the number of unperturbed electron states is restricted with only 12 with a given value $K = 1$ for each state. It is, therefore, clear that no other value of K could appear as a quantum number of the electron states. In this sense the conservation of $\mathbf{K}^2$ is also trivial, similarly to the conservation of $\mathbf{I}^2$ and $\mathbf{S}^2$, which has been pointed out before.

Let us briefly discuss the structure of the two ground states depending on the acceptor position inside the nanocrystal, and the nanocrystal size. The acceptor position in the dot, i.e. the parameter $q = h/R$, influences the magnitude of the s–p Coulomb matrix element $V(q) = \sqrt{V_x^2(q) + V_y^2(q) + V_z^2(q)}$, as is shown in figure 3. The dot radius R defines the spacing between the unperturbed energy levels, shown in figure 1, as R^{-2}. At the same time $V(q)$ falls proportionally to R^{-1} as R increases; see figure 3. If $E_{1h}(q) - E_{0h}(q) \gg V(q)$, then $\cos\beta \to 1$ and $\sin\beta \to 0$. This means that the ground states remain predominantly the states with the s-type envelope function, i.e. $l = 0$ for these states, as in the cases of no impurity in the dot or centrally located impurity. In contrast, if $E_{1h}(q) - E_{0h}(q) \ll V(q)$, then $\cos\beta \to \sin\beta \to 1/\sqrt{2}$. In this case the s-type and p-type envelope functions have equal 'weights' in the ground states. Thus, the quota of the s-type envelope function asymptotically reduces to 0.5 as the ratio $V(q)/(E_{1h}(q) - E_{0h}(q))$ increases. It is possible to calculate this quota as the probability $P = \cos^2\beta$ for being in the ground state with the s-type envelope function. Its dependence on the dimensionless magnitude of the acceptor position vector q for different dot radii is presented in figure 4 (upper panel). It is seen that the greater values of P are achieved at smaller values of the dot radius (correspondingly, greater values of $E_{1h}(q) - E_{0h}(q)$) and smaller values of q, which provide the smaller values of $V(q)$. If the acceptor is located at the dot centre ($q = 0$), then the quota of the s-type envelope function equals 1. In the opposite case, when the dot radius becomes greater, and q corresponds to the maximum of $V(q)$ (see figure 3), the probability approaches 0.5.

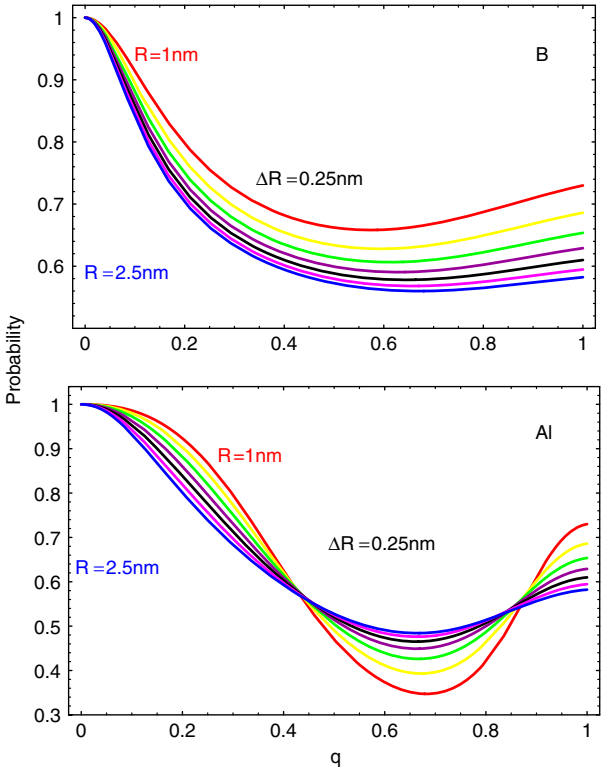

Figure 4. 'Weight' of the s-type envelope function in the ground state of B (upper panel) and Al (lower panel) doped dots as functions of the dimensionless acceptor displacement $q = h/R$ at various dot radii from 1 to 2.5 nm with the step ΔR shown in the figure.

The energies of the other states are determined as the solutions of the fourth-order algebraic equation

$$(E - E_{0h}^{(0)}(q))(E - E_{0h}^{(1)}(q))(E - E_{1h}^{(0)}(q))(E - E_{1h}^{(1)}(q)) = \frac{V^2(q)}{2}(E - E_{0h}(q))(E - E_{1h}(q)) \quad (22)$$

that is solved numerically. As follows from an explicit form of $E_{0,4}$ and equation (22), the energies of all the six doublets depend exclusively on the distance between the dot centre and impurity, and do not depend on the **h** direction. According to, at least, equations (19) and (20) this circumstance does not take place for the wavefunctions.

Dependences of all the six energies, including the energies $E_{0,4}$, on the dot radius and the dimensionless magnitude q of the acceptor position vector are shown in the upper panels of figures 5 and 6, respectively. As has been pointed out previously, boron may be treated as a hydrogenic acceptor, because $Q = 0$ and the central cell correction is absent. Therefore, the curves plotted in the upper panels may be applied to boron as has been indicated in the figures. All the energies in both figures are counted from the mean quadruplet energy $(E_{0h}^{(0)}(q) + E_{1h}^{(0)}(q))/2$.

The dependence on the dot radius is monotonic for all the energies, while the dependences on the dimensionless displacement q are essentially more complicated. Indeed, as is seen in the figures, the energy level E_0 (lowest solid line) always remains the lowest one and represents the energy of the two ground states. At $q \to 0$ this level interflows with the level E_1, obtained as the lowest solution of equation (22), which leads to the formation of the s-type quadruplet with the energy $E_{0h}^{(0)}(0)$. Formation of the p-type quadruplet with the energy $E_{1h}^{(0)}(0)$ at $q \to 0$ is a result of a junction of the level E_4 and the level E_3 being the third solution of equation (22), as follows from figure 6. It is also seen that maximal splitting of the spectrum is achieved at approximately $q = 0.46$ which corresponds to the maximal values of the s–p-type Coulomb matrix element $V(q)$; see figure 3.

The spatial distribution of the hole density for all the six doublets is shown in figure 7 for two values of q: $q = 0.1$ (left column) and $q = 0.46$ (right column). In fact, we have plotted the average of the squared absolute value of the total wavefunction over the unit cell. In this case the Bloch function oscillations do not appear in the electron density that reduces to the 'density of envelope function'

$$\rho_{\mathrm{env}}(\mathbf{r}) = \sum_{j=1}^{6} |\Phi_j(\mathbf{r})|^2, \quad (23)$$

where $\Phi_j(\mathbf{r})$ is the jth element of the 6D envelope function vector $|\Phi\rangle$ as before. It is worth emphasizing that the functions $\rho_{\mathrm{env}}(\mathbf{r})$ for two different 6D vectors within any doublet turn out to be the same. This is a consequence of the twofold degeneracy, taking place for any doublet, having, in fact, spin nature. Since we are interested only in the spatial distribution of the envelope function density, one may calculate $\rho_{\mathrm{env}}(\mathbf{r})$ with any of the two 6D vectors of the doublet.

As our calculations show, for all six doublets the envelope function density has an axial symmetry with respect to the line drawn through the dot centre and acceptor. Therefore $\rho_{\mathrm{env}}(\mathbf{r})$ has the same distribution in any dot cross-section to which the acceptor position vector belongs. We have depicted in figure 7 such a central cross-section of the electron density averaged over the unit cell (in the sense of equation (23)) for all the doublets. Brighter areas in the density plots correspond to higher values of $\rho_{\mathrm{env}}(\mathbf{r})$. The circle represents the nanocrystal boundary, and the bold point, situated at the vertical axis, indicates the acceptor location. Since the distribution picture is of axial symmetry related to the acceptor position vector,

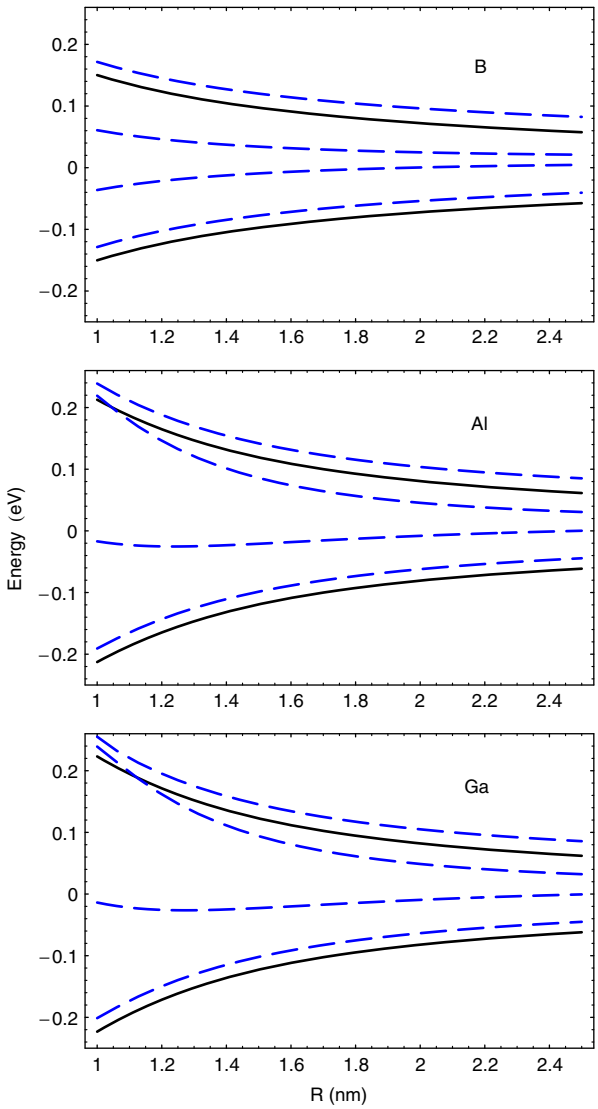

Figure 5. Splitting of the two lower hole levels shown in figure 1 into the six doublet levels under the action of the spin–orbit and Coulomb interactions for the dots doped with: hydrogen-like (boron) acceptors—upper panel; and real acceptors, such as Al—middle panel, and Ga—lower panel. The Coulomb field of the real acceptors includes not only the long range part of the hydrogen-like kind, which is typical for boron, but also the short range term that considerably enhances the energy splitting. Solid lines represent the doublet energies described by equation (18), for boron, and (25), for aluminium and gallium (see the text). Dashed lines are the solutions of the fourth-order equations (22), for boron, and (26), for aluminium and gallium.

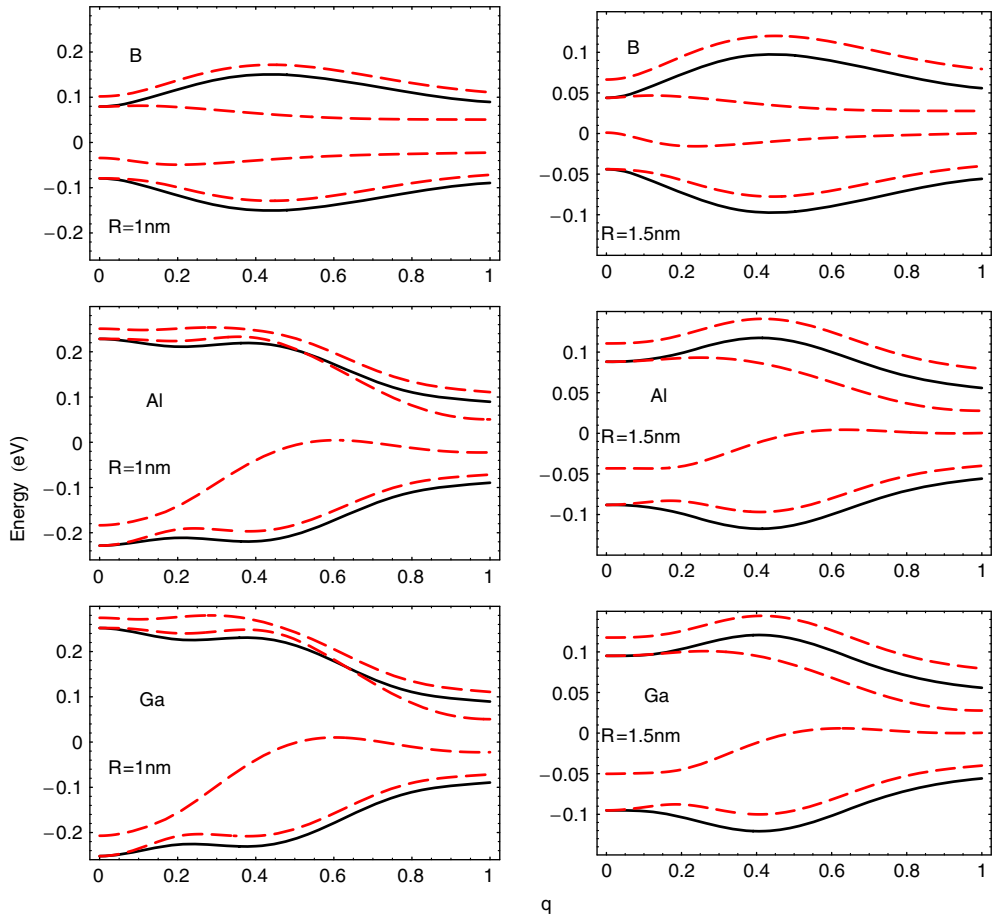

Figure 6. Hole spectra of the doped dot as functions of the dimensionless acceptor displacement $q = h/R$ from the dot centre. The direction of the acceptor position vector **h** is defined by $h_x/h = 0.8$, $h_y/h = 0.5$, and $h_z/h = 0.33$. Dashed and solid lines imply the same as those in figure 5 (see the caption).

such an acceptor position may be treated as an arbitrary one, without loss of generality.

To illustrate the role of the system asymmetry due to acceptor existence in the dot, we have chosen two values of the acceptor displacement from the dot centre. The first one, $q = 0.1$, defines weak deviations from the central symmetric picture in the electron density distribution taking place at $q = 0$. The second value, $q = 0.46$, corresponds to the greatest magnitude of the s–p-type Coulomb matrix element $V(q)$ and, consequently, the maximal degree of the system asymmetry.

It should be noted that general trends in a relocation of the electron density under the action of the acceptor electric field are, in fact, similar for all the doublets in both cases $q = 0.1$ and $q = 0.46$. In particular, the ground state electron density shifts to the acceptor site, while for the excited states, as the energy of the state increases, the electron density gradually moves into the areas free of the acceptor.

It is also interesting to trace some correlation between the energy level behaviour (see figure 6) and the envelope function density depending on q. As is seen in figure 6, for all values of q, except for the small values not exceeding $q \sim 0.2$, the energy branches E_0 and E_1, as well as E_4 and E_5, are close and parallel. This indicates, presumably, that the electron densities should resemble each other, which is confirmed by the panels (a), (b), and (e), (f) in the right column of figure 7. At small q the level E_1 is very close to the energy level of the ground states E_0, but does not 'interact' with it. As a result, the wavefunctions and the electron densities of these doublets appreciably differ; see panels (a) and (b) in left column of figure 7. At the same time, the plots in the left panels (b) and (c) almost coincide. Figure 6 shows that as q increases from zero, the levels E_1 and E_2 converge, forming anticrossing at $q \approx 0.1$. This indicates the greater interaction between these two levels compared to that with all the other levels. However both these levels are of the s type at $q \to 0$. Therefore, the squared absolute values of the corresponding wavefunctions turn out to be almost the same, as shown in the plots (b) and (c). The strongly excited states with the energies E_3, E_4, and E_5 are constructed predominantly from the states with the p-type envelope functions, which yields asymmetric pictures of the density distributions.

Finally, we touch briefly on the envelope function density in the nanocrystal at $q = 1$. The s–p Coulomb matrix elements have some intermediate values in this case, see figure 3, relative to the cases considered above. Hence, one could expect for $q = 1$ the distribution picture being a transient one between the pictures presented in the left and right panels of figure 7.

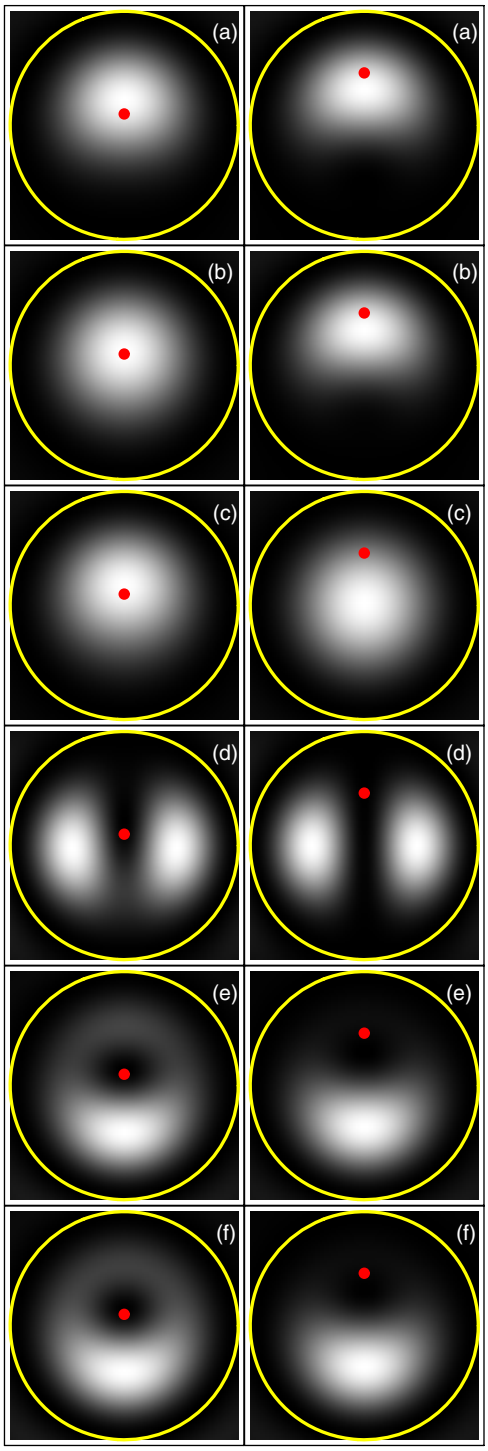

Figure 7. Density plot of the probability distribution $\rho_{\rm env}(\mathbf{r})$ of all the six doublets at $q = 0.1$ (left column), and $q = 0.46$ (right column) for a nanocrystal's central cross-section containing the hydrogenic (boron) acceptor. The acceptor position is indicated with a bold point. (a)—ground state; from (b) to (f)—from first to fifth excited states. For each state the hole density is normalized to its maximum in this state, and rises from dark to light. The nanocrystal boundary is shown with the circle. $R = 1.5$ nm.

Meanwhile, the calculations show that the electron density in this case is almost equivalent to that at $q = 0.46$. For this reason we do not depict it in figure 7. Such conformity is explained, presumably, with approximate invariance for $q \geqslant 0.46$ of the basic parameter $V(q)/(E_{1\rm h}(q) - E_{0\rm h}(q))$ defining the spectrum splitting.

4.2. Central cell effect

Let us now examine the role of the central cell field in the fine structure formation in silicon nanocrystals doped with some other acceptors of the third group, such as aluminium and gallium. In contrast to boron, all these chemical elements produce a substantial chemical shift of the ground state energy in bulk silicon. Therefore, we may expect considerable reconstruction of the energy spectrum and hole states in the dots with these acceptors. We shall not consider the nanocrystals doped with indium and, especially, thallium because they are deep impurities rather than the shallow ones. For this reason the acceptor states in In and Tl doped dots will mainly form under the action of the acceptor field but not the confining potential of the dot. Meanwhile, our treatment implies the opposite.

Formally, the basic equation of the eigenstate and eigenvalue problem (equation (17)) does not change its form in the case where we take into account the central cell field. However potential energy $V(\mathbf{r})$ has now a short range nonzero addition $\bar{W} = -Q\delta(\mathbf{r} - \mathbf{h})$ that can be comparable with the long range part $V_{\rm sp}(r) + V_{\rm ih}(\mathbf{r}, \mathbf{h})$ of the Coulomb field. Correspondingly, matrix elements of $\bar{W}$ arise in equation (17) and produce changes in the solutions obtained earlier for the case of a hydrogenic (boron) acceptor. The s–s, s–p, and p–p matrix elements of the averaged central cell potential $\bar{W}$ have the following form:

$$\begin{aligned}
\langle s|\,\bar{W}|s\rangle &= -Q\frac{\pi j_0^2(\pi q)}{2R^3} \equiv W_{\rm ss}(q),\\
\langle s|\,\bar{W}|p_a\rangle &= -Q\frac{\sqrt{3}\,j_0(\pi q)\,j_1(\mu q)n_a}{2R^3\,j_0(\mu)} \equiv W(q)n_a, \qquad (24)\\
\langle p_a|\,\bar{W}|p_b\rangle &= -Q\frac{3j_1^2(\mu q)n_a n_b}{2\pi R^3\,j_0^2(\mu)} \equiv W_{\rm pp}(q)n_a n_b,
\end{aligned}$$

where $n_a = h_a/h$, and $j_0(x)$, $j_1(x)$ are the spherical Bessel functions of the argument x.

As before, equation (17) yields two doublet and two quadruplet solutions. The energies of the doublet states are obtained analytically and represent the energies of the ground and third or fourth excited states, as shown in figure 6 with solid lines. The explicit form of the doublet energies is as follows:

$$\begin{aligned}
E_{0,3/4} = {} & \frac{E_{0\rm h}^{(0)}(q) + E_{1\rm h}^{(0)}(q) + W_{\rm ss}(q) + W_{\rm pp}(q)/2}{2}\\
& \pm\tfrac{1}{2}[(E_{0\rm h}^{(0)}(q) - E_{1\rm h}^{(0)}(q) + W_{\rm ss}(q) - W_{\rm pp}(q)/2)^2\\
& + 2(V(q) + W(q))^2]^{1/2}. \qquad (25)
\end{aligned}$$

Here we employ the notation $E_{3/4}$ for the upper doublet energy, because at small R, depending on q and R, see figures 5 and 6 (left column), it corresponds to either the third or the fourth excited state. The quadruplet energies are obtained as solutions

of the fourth-order equation

$$(E - E_{0h}^{(0)}(q) - W_{ss}(q))(E - E_{0h}^{(1)}(q) - W_{ss}(q)) \times [(E - E_{1h}^{(0)}(q))(E - E_{1h}^{(1)}(q)) - W_{pp}(q) \times (E - E_{1h}(q))/2] = \frac{(V(q) + W(q))^2}{2}(E - E_{0h}(q) - W_{ss}(q)) \times (E - E_{1h}(q)). \quad (26)$$

Of course, expressions (25) and (26) transform into the above expressions (18) and (22), respectively, if the central cell matrix elements vanish.

It is possible to consider the energies E_j, as well as the matrix elements of both the short and long range parts of the Coulomb interaction, as functions of the two arguments: dimensionless impurity displacement q, and dot radius R. If q = const, matrix elements of the short range potential decrease proportionally to R^{-3} as R increases. Matrix elements of the long range part decrease more slowly, as R^{-1}. At small dot sizes, of about 2 nm, the central cell corrections turn out to be the main factor influencing the dot spectrum, while for bigger dots, having sizes of the order of 4–5 nm, the central cell corrections are sharply reduced. The hole spectra for Al and Ga are shown in figure 5 (two lower panels) depending on R at $q = 0.46$. It is seen that the spectra are very similar. This has a simple explanation. Parameters Q for Al and Ga are very close ($Q_{Ga}/Q_{Al} = \eta_{Ga}/\eta_{Al} = 1.155$), which leads to the similarity in the central cell potentials of these dopants, and the energy spectra of the dot. As is seen in the figure, the energy splittings for 2–3 nm nanocrystals are remarkably different for B, and Al and Ga. The strong central cell field provides the greater splitting in the spectrum relative to the case of the boron acceptor. At the same time, in the range of the dot radius 2–2.5 nm, the energy spectra of the dot with Ga and Al become very similar to the spectrum of the B doped dot. This, indeed, indicates significant weakening of the central cell corrections for 4–5 nm quantum dots. Apparently, the long range Coulomb field becomes even more extensive at $R \sim$ 2–2.5 nm than the short range one.

The dependence of the Coulomb matrix elements of both kinds on q at fixed R has more complicated character (see figure 3). This dependence defines some nonmonotone behaviour of the energy branches as functions of q. The picture of the energy splitting versus the dimensionless displacement q for Al and Ga doped dots is presented in figure 6 (two lower panels in both columns) for two values of the dot radius. All the levels remain doubly degenerate. This is a consequence of the absence of magnetic field in the system.

In the case of the central located acceptor in the Al or Ga doped dot, the s- and p-type levels strongly diverge from each other compared to the case for the B doped dot, see figure 6, on the distance mainly determined by the s–s-type matrix element $W_{ss}(0)$. The matrix element $W_{ss}(q)$ has its maximal value at $q = 0$, and the s-type level shifts down by a magnitude of $W_{ss}(0)$. At the same time $W_{pp}(0) = 0$, and the p-type level stays at its primary position. Since the s–p matrix elements of both the short and long range parts of the Coulomb interaction equal zero as well, the s- and p-type levels do not mix, which leads to the existence of uncoupled s- and p-type doublets and s-and p-type quadruplets, as shown in figure 6. Naturally, the divergence of the s- and p-type levels becomes greater for the dots of smaller sizes, and for acceptors with more extensive short range Coulomb interaction.

We can compare our results on the energy splitting for the central located boron, aluminium, and gallium acceptors with the ones obtained earlier by Zhou *et al* [2] within the frames of the local density approximation. Note, however, that their calculations have been performed for a nanocrystal with too small a size, about 1.6 nm according to the authors' estimations. Applicability of the $\mathbf{k} \cdot \mathbf{p}$ method for such small nanocrystals is, of course, questionable. Nevertheless, we have determined the energy splitting for a 1.6 nm nanocrystal by the method used in the present paper. Quite good agreement has been found between the results of our works. In particular, we have obtained the difference of the p-type quadruplet and the s-type doublet energies approximately equal to 0.2 eV (B), 0.75 eV (Al), and 0.85 eV (Ga), while according to [2] these energies, respectively, equal 0.25, 0.55, and 0.55 eV. Perhaps some remarkable excess of the energy values arising in our calculations for Al and Ga can be explained by the sufficiently crude approximation used for the determination of parameter Q, and too small size of the 'test' nanocrystal. Since the short range Coulomb matrix elements sharply increase as the dot size decreases (as R^{-3}), any, even small, error in the value of Q can be enhanced at small R. This allows one to hope that for bigger dots, which are considered in the present work, our results could be applied with greater accuracy.

As q gradually increases, the s–p Coulomb matrix elements increase as well and achieve their maximum at approximately $q \sim$ 0.4–0.5. Accordingly, strong coupling of the s-and p-type hole states and significant reconstruction of the energy spectrum take place at those values of q. Further increase of q leads to the fast reduction of all the short range Coulomb matrix elements which equal exactly zero at the nanocrystal boundary. As a result, the orders of the energy levels at $q = 1$, and their energies, are the same for all the dopants.

To compare the hole densities in the nanocrystal with embedded hydrogen-like and real acceptors we have plotted in figure 8 the difference of the envelope function densities for Al and B: $\Delta\rho(\mathbf{r}) = \rho_{env}^{(Al)}(\mathbf{r}) - \rho_{env}(\mathbf{r})$ for $R = 1.5$ nm. The wavefunctions and hole densities of the Ga doped quantum dot are almost equivalent to those of the Al doped dot. All the distinctions can be estimated to a few per cent. For this reason we do not adduce here corresponding plots for gallium. The envelope function density $\rho_{env}^{(Al)}(\mathbf{r})$ has again an axial symmetry as it had earlier for the case of the hydrogen-like acceptor. The left column in figure 8 shows $\Delta\rho(\mathbf{r})$ for $q = 0.1$. $\Delta\rho(\mathbf{r})$ for $q = 0.46$ has been shown in the right column.

There are seen in figure 8 (left column) the general trends in behaviour of the hole densities at small q that may be formulated as follows. All the states, having lower energies compared to the corresponding energies of the B doped dot, tend to have additional accumulation of the hole density at the acceptor site. Naturally, the states with the higher energies have an opposite trend. At the same time, as follows from our calculations, the absolute value of $\Delta\rho(\mathbf{r})$ for any state is

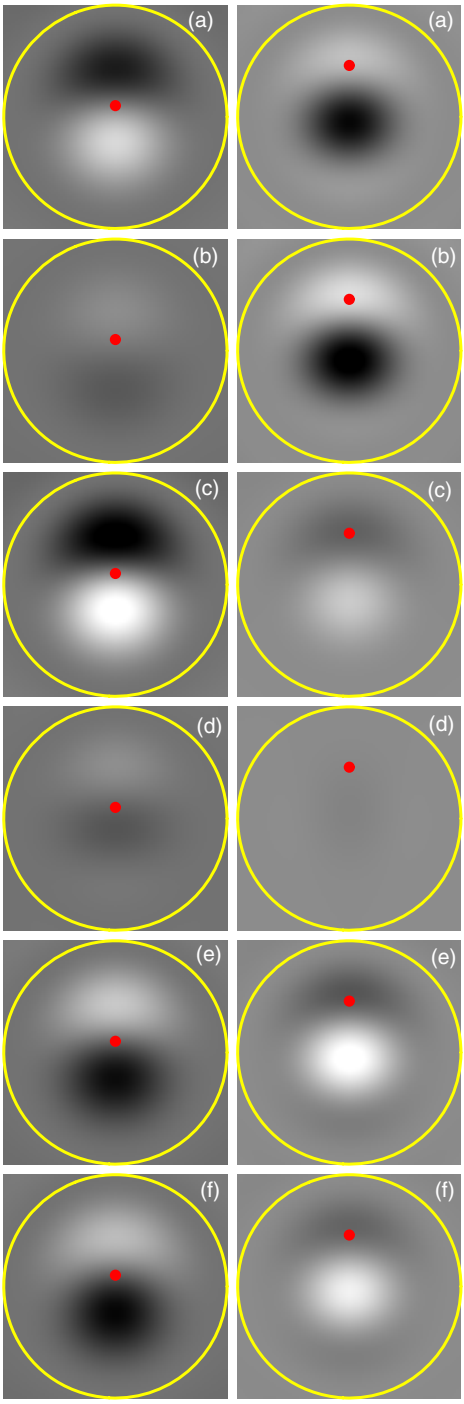

Figure 8. Density plot of $\Delta\rho(\mathbf{r})$ caused by the central cell potential of the Al dopant in a 3 nm nanocrystal. Dark and light areas correspond to minimal negative and maximal positive values, respectively, of $\Delta\rho(\mathbf{r})$. The unit of the grayscale bar is the same for all panels. Left column—$q = 0.1$, right column—$q = 0.46$. The circle shows the boundary of the dot's central cross-section containing the acceptor. The latter is indicated with a bold point.

of the order of ten per cent of $\rho_{\text{env}}(\mathbf{r})$ or even less. Hence, one may conclude that the relocation of the hole density caused by the short range Coulomb field remains sufficiently weak. Accordingly, the short range field does not lead to the considerable reconstruction of the hole states.

The appearance of some additional hole density near the acceptor is also confirmed with figure 4 (lower panel) for the ground state. Obviously, the shift of the hole density from the dot boundary to the acceptor leads to the probability distribution becoming predominantly of the 's' type. This should give an increase of the quota of the s-type envelope function in the ground state doublet, which is actually seen in figure 4. At $q = 0.1$ the probability of having the s-type envelope function for the Al doped dot is greater than that for the B doped dot. However, the situation reverses as q increases. For instance, the s-type envelope function 'weight' reduces in the ground state doublet for $q = 0.46$ in the dot with aluminium relative to the dot with boron as shown in figure 4.

At $q = 0.46$, functions $\Delta\rho(\mathbf{r})$ for the ground and first excited states, see figure 8 (right column, panels (a) and (b)), become positive around and above the acceptor on the dot cross-section, and negative below the impurity. However, it is seen in figure 7, panels (a) and (b), that the maxima of the hole densities at $q = 0.46$ are located a little below the acceptor, between the latter and the dot centre, in contrast to the case for $q = 0.1$ (panels (a) and (b) of the left column in figure 7). Hence, the envelope function density again shifts towards the acceptor. This means that the redistribution of the hole density inside the nanocrystal in the case where $q = 0.46$, in fact, obeys the previous regularity: the hole density tends to collect near the acceptor due to the additional short range potential. Naturally, an opposite trend is observed for the highly excited states, the fourth and fifth ones. As in the case of $q = 0.1$, we emphasize that all the changes remain very weak and do not exceed several per cent of $\rho_{\text{env}}(\mathbf{r})$.

5. Conclusion

Now we briefly summarize our consideration with a few concluding remarks. First, it has been revealed that introduction of a shallow acceptor inside a silicon nanocrystal leads to the total removal of the spectrum degeneracy, except for the twofold spin degeneracy that can be removed only with a magnetic field. The structure obtained for the spectrum strongly depends on what chemical element is embedded into the quantum dot. The level splitting increases for the acceptors with stronger central cell interaction. It is not so for the wavefunctions. They change insignificantly, and within accuracy of ten per cent may be described using the functions of the dot doped with a hydrogenic acceptor. Second, we have found the dependence of the energy splitting on the dot size. The splitting gradually increases if the dot size decreases. Finally, the energy spectrum has a complicated pattern depending on the acceptor position in the dot. In particular, for Al and Ga doped dots, maximal splitting of the levels takes place at small acceptor displacement from the dot centre, while for hydrogen-like impurity the splitting becomes maximal at the distances of about half the dot radius. At the same time, maximal reconstruction of the dot spectrum, accompanied by the maximal entanglement of all the states, always takes place at about $R/2$ displacement, especially for small nanocrystal sizes.

Acknowledgments

We thank the Russian Ministry of Education and Science, and the Russian Foundation for Basic Research for the financial support of our work through the programme 'Development of scientific potential of the high school' (the project 2.1.1.2363), and the project 05-02-16762, respectively.

References

[1] Melnikov D V and Chelikowsky J R 2004 *Phys. Rev. Lett.* **92** 046802
[2] Zhou Z, Steigerwald M L, Friesner R A, Brus L and Hybertsen M S 2005 *Phys. Rev.* B **71** 245308
[3] Xu Q, Luo J W, Li S S, Xia J B, Li J and Wei S H 2007 *Phys. Rev.* B **75** 235304
[4] Belyakov V A and Burdov V A 2007 *Phys. Lett.* A **367** 128
[5] Belyakov V A and Burdov V A 2007 *Phys. Rev.* B **76** 045335
[6] Fujii M, Mimura A, Hayashi S and Yamamoto K 1999 *Appl. Phys. Lett.* **75** 184
[7] Mimura A, Fujii M, Hayashi S, Kovalev D and Koch F 2000 *Phys. Rev.* B **62** 12625
[8] Tetelbaum D I, Trushin S A, Burdov V A, Golovanov A I, Revin D G and Gaponova D M 2001 *Nucl. Instrum. Methods* B **174** 123
[9] Fujii M, Mimura A, Hayashi S, Yamamoto Y and Murakami K 2002 *Phys. Rev. Lett.* **89** 206805
[10] Fujii M, Toshikiyo K, Takase Y, Yamaguchi Y and Hayashi S 2003 *J. Appl. Phys.* **94** 1990
[11] Fujii M, Yamaguchi Y, Takase Y, Ninomiya K and Hayashi S 2004 *Appl. Phys. Lett.* **85** 1158
[12] Kachurin G A, Cherkova S G, Volodin V A, Kesler V G, Gunakovsky A K, Cherkov A G, Bublikov A V and Tetelbaum D I 2004 *Nucl. Instrum. Methods* B **222** 497
[13] Mikhaylov A N, Tetelbaum D I, Burdov V A, Gorshkov O N, Belov A I, Kambarov D A, Belyakov V A, Vasiliev V K, Kovalev A I and Gaponova D M 2007 *J. Nanosci. Nanotechnol.* to be published
[14] Tsu R and Babic D 1994 *Appl. Phys. Lett.* **64** 1806
[15] Lannoo M, Delerue C and Allan G 1995 *Phys. Rev. Lett.* **74** 3415
[16] Allan G, Delerue C, Lannoo M and Martin E 1995 *Phys. Rev.* B **52** 11982
[17] Tsu R, Babic D and Ioriatti L 1997 *J. Appl. Phys.* **82** 1327
[18] Bassani F, Iadonisi G and Preziosi B 1974 *Rep. Prog. Phys.* **37** 1099
[19] Bernholc J and Pantelides S T 1977 *Phys. Rev.* B **15** 4935
[20] Pantelides S T 1978 *Rev. Mod. Phys.* **50** 797
[21] Lipari N O and Baldereschi A 1978 *Solid State Commun.* **25** 665
[22] Lipari N O, Baldereschi A and Thewalt M L W 1980 *Solid State Commun.* **33** 277
[23] Kohn W and Luttinger J M 1955 *Phys. Rev.* **97** 1721
[24] Kohn W and Luttinger J M 1955 *Phys. Rev.* **98**
[25] Ogut S, Burdick R, Saad Y and Chelikowsky J R 2003 *Phys. Rev. Lett.* **90** 127401
[26] Delerue C, Lannoo M and Allan G 2003 *Phys. Rev.* B **68** 115411
[27] Cartoixa X and Wang L W 2005 *Phys. Rev. Lett.* **94** 236804
[28] Trani F, Ninno D, Cantele G, Iadonisi G, Hameeuw K, Degoli E and Ossicini S 2006 *Phys. Rev.* B **73** 245430
[29] Delerue C and Lannoo M 2004 *Nanostructures: Theory and Modelling* (Berlin: Springer)
[30] Babic D, Tsu R and Greene R F 1992 *Phys. Rev.* B **45** 14150
[31] Takagahara T and Takeda K 1992 *Phys. Rev.* B **46** 15578
[32] Ferreyra J M and Proetto C R 1999 *Phys. Rev.* B **60** 10672
[33] Burdov V A 2002 *Zh. Eksp. Teor. Fiz.* **121** 480
Burdov V A 2002 *JETP* **94** 411 (Engl. Transl.)
[34] Feng D H, Xu Z Z, Jia T Q, Li X X and Gong S Q 2003 *Phys. Rev.* B **68** 035334
[35] Moskalenko A S and Yassievich I N 2004 *Fiz. Tverd. Tela* **46** 1465
Moskalenko A S and Yassievich I N 2004 *Phys. Solid State* **46** 1508 (Engl. Transl.)
[36] Hada Y and Eto M 2003 *Phys. Rev.* B **68** 155322
[37] Blom A, Odnoblyudov M A, Yassievich I N and Chao K A 2003 *Phys. Rev.* B **68** 165338
[38] Baldereschi A and Lipari N O 1973 *Phys. Rev.* B **8** 2697
[39] Baldereschi A and Lipari N O 1974 *Phys. Rev.* B **9** 1525
[40] Voos M, Uzan P, Delalande C, Bastard G and Halimaoui A 1992 *Appl. Phys. Lett.* **61** 1213
[41] Luttinger J M 1956 *Phys. Rev.* **102** 1030
[42] Efros A L and Rodina A V 1989 *Solid State Commun.* **72** 645
[43] Grigoryan G B, Kazaryan E, Efros Al L and Yazeva T V 1990 *Fiz. Tverd. Tela* **32** 1772
Grigoryan G B, Kazaryan E, Efros Al L and Yazeva T V 1990 *Sov. Phys.—Solid State* **32** 1031 (Engl. Transl.)
[44] Efros A L 1992 *Phys. Rev.* B **46** 7448
[45] Fonoberov V A, Pokatilov E P and Balandin A A 2002 *Phys. Rev.* B **66** 085310
[46] Zhu Y H, Zhang X W and Xia J B 2006 *Phys. Rev.* B **73** 165326